Single Task Optimization-Based Planar Box Delivery Motion Simulation and Experimental Validation

Yujiang Xiang[1]
Department of Mechanical and Aerospace Engineering,
Oklahoma State University,
Stillwater, OK 74078
e-mail: yujiang.xiang@okstate.edu

Shadman Tahmid
Department of Mechanical Engineering,
Texas Tech University,
Lubbock, TX 79409
e-mail: shadman.tahmid@ttu.edu

Paul Owens
Department of Mechanical Engineering,
University of Alaska Fairbanks,
Fairbanks, AK 99775
e-mail: pdowens@alaska.edu

James Yang
Department of Mechanical Engineering,
Texas Tech University,
Lubbock, TX 79409
e-mail: james.yang@ttu.edu

Box delivery is a complicated task and it is challenging to predict the box delivery motion associated with the box weight, delivering speed, and location. This paper presents a single task-based inverse dynamics optimization method for determining the planar symmetric optimal box delivery motion (multi-task jobs). The design variables are cubic B-spline control points of joint angle profiles. The objective function is dynamic effort, i.e., the time integral of the square of all normalized joint torques. The optimization problem includes various constraints. Joint angle profiles are validated through experimental results using root-mean-square-error (RMSE) and Pearson's correlation coefficient. This research provides a practical guidance to prevent injury risks in joint torque space for workers who lift and deliver heavy objects in their daily jobs. [DOI: 10.1115/1.4049647]

Keywords: box delivery, lifting, carrying, transition, injury risks, inverse dynamic optimization, control, dynamics, mobile robots

1 Introduction

Manual material handling tasks are still common in various industries and production systems, and all will remain the same in the near future although emerging assistive devices are on the way. Although significant research efforts have been devoted to reducing the number and severity of manual material handling injuries it is still a burden on industries that the direct costs are over $13 billion in 2016 in the USA [1]. Many industrial work processes include multi-task jobs (e.g., box delivery that involves box lifting, carrying and lowering it). In multi-task case, workers combine subtasks with transition phases, which affect workers' pace, posture, motion, and joint load [2]. Digital human modeling provides a useful tool for researchers to investigate the cause and effect without worrying about injuries. However, simulation of a human delivering task proves to be a challenging problem from an analytical and computational point of view. The primary goal of this study is to explore an inverse dynamic optimization formulation to predict and analyze dynamic human delivering motion in ergonomic applications. The simulation needs to be computationally efficient in an effort to provide real-time implementation.

In digital human modeling simulation, the box delivery task could be considered as one single task; therefore, it can be formulated as one single inverse dynamic optimization problem. There is extensive literature on the study of lifting and carrying motions. In addition, the task decomposition method was used to simulate gait motion with single support and double support phases [3], but few studies have been conducted on the delivering task (multi-task jobs). The optimization formulation for dynamic human motion planning could be roughly divided into five categories: forward dynamic simulation [4–10], inverse dynamic simulation [11–17], collocation method [18,19], control-based method [20–24], and mixed formulation method [25–27]. Forward dynamic simulation can accurately describe the law of physics through integration of equations of motion (EOM) using small time-step. However, it usually takes more computation time. In contrast, inverse dynamic method only evaluates EOM at discretized time nodal points, and collocation method only sets up equality constraints of EOM at time nodal points. For these two methods, the law of physics is related to the number of time nodal points used to discretize the problem. Furthermore, mixed formulations are proposed in the literature to achieve better performance by taking advantage of different simulation methods, such as computed muscle control which uses forward dynamic simulation and feedback control [26,27].

In this study, the inverse dynamic optimization is adopted for two-dimensional (2D) box delivery simulation. This method has some advantages over forward dynamic simulation in terms of computational efficiency, this is because EOM is directly evaluated from inverse dynamics in each optimization iteration.

The objective of this study is to explore the method that can generate motion from start to finish of a delivery task by using single task-based approach and experimental validation. The contributions of this study are as follows: (1) This work is the first study of predictive object delivery formulation in the literature and it is the first step to investigate the complete delivery motion formulation, which sets up a solid foundation to understand the delivery task and to investigate the formulation for future research using three-dimensional musculoskeletal models and (2) the proposed predictive delivery formulation does not depend on experimental data. Previous works are mainly empirical studies based on experimental data, i.e., data-drive approach [28].

The rest of this paper is organized as follows. The skeletal human system is first described in Sec. 2, and EOM is also detailed. Section 3 is motion capture experiment. Section 4 covers the details of the single task-based optimization formulation for box delivery problem and box delivery simulation results are presented in Sec. 5. Finally, discussion and conclusion are given in Sec. 6.

2 2D Skeletal Human Model

A 2D skeletal model with 14 degrees of freedom (DOFs) defined in joint space is used to simulate symmetric delivery motion, as shown in Fig. 1. Three DOFs are used for global translation (y, z) and rotation (β), and 11 DOFs (q_1, q_2, $\ldots q_{11}$) are used for the human body joints. The global DOFs are composed of two translational (prismatic) joints and one rotational (revolute) joint. The legs and arms are assumed to be symmetric. There are three branches in the body frame with respect to the global coordinate branch: one

[1]Corresponding author.

Contributed by the Mechanisms and Robotics Committee of ASME for publication in the Journal of Mechanisms and Robotics. Manuscript received October 2, 2019; final manuscript received December 11, 2020; published online February 23, 2021. Assoc. Editor: Chin-Hsing Kuo.

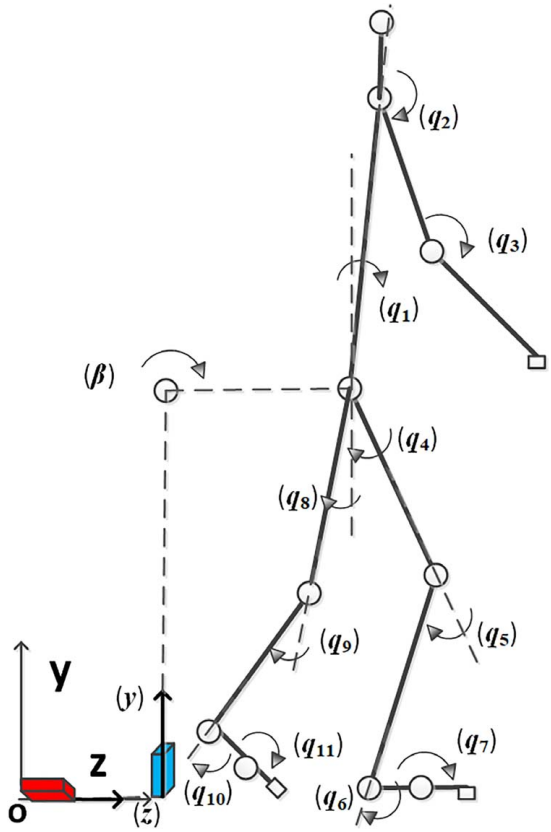

Fig. 1 The 2D skeletal model

spine-arm branch and two leg branches. In the spine-arm branch, two arms are represented as a single branch, since only 2D symmetric motion in sagittal plane is studied. The arm branch includes upper arm and lower arm. Each leg consists of a thigh, a shin, a hinder foot, and a forefoot. The 50th percentile anthropometric data for the skeletal model is generated using GEBOD software [29].

Figure 1 depicts how the DOFs are set up in the Denavit-Hartenberg method [30]. The DOF is given in the local z-direction in each joint. The global rotation joint (β), spine joint (q_1), and two hip joints (q_4 and q_8) coincide at the same location. The positive directions for all the rotation joints ($q_1 - q_{11}$) are clockwise in the global Y–Z plane. A recursive Lagrangian dynamics formulation is used for this model, and the ground reaction force is calculated from an inverse procedure based on joint kinematics, gravity, and external loads. The details are presented in Xiang et al. [31]. The forward joint kinematics are calculated as

$$\mathbf{A}_i = \mathbf{T}_1\mathbf{T}_2\mathbf{T}_3\cdots\mathbf{T}_i = \mathbf{A}_{i-1}\mathbf{T}_i \tag{1}$$

$$\mathbf{B}_i = \dot{\mathbf{A}}_i = \mathbf{B}_{i-1}\mathbf{T}_i + \mathbf{A}_{i-1}\frac{\partial \mathbf{T}_i}{\partial q_i}\dot{q}_i \tag{2}$$

$$\mathbf{C}_i = \dot{\mathbf{B}}_i = \ddot{\mathbf{A}}_i = \mathbf{C}_{i-1}\mathbf{T}_i + 2\mathbf{B}_{i-1}\frac{\partial \mathbf{T}_i}{\partial q_i}\dot{q}_i + \mathbf{A}_{i-1}\frac{\partial^2 \mathbf{T}_i}{\partial q_i^2}\dot{q}_i^2 + \mathbf{A}_{i-1}\frac{\partial \mathbf{T}_i}{\partial q_i}\ddot{q}_i \tag{3}$$

where q_i is the ith joint angle, $\mathbf{T}_i$ is the link transformation matrix from the $(i-1)$th link frame to the ith link frame, and $\mathbf{A}_0 = [\mathbf{I}]$, $\mathbf{B}_0 = \mathbf{C}_0 = [\mathbf{0}]$.

The backward joint torque equations are defined as follows,

$$\tau_i = tr\left(\frac{\partial \mathbf{A}_i}{\partial q_i}\mathbf{D}_i\right) - \mathbf{g}^T\frac{\partial \mathbf{A}_i}{\partial q_i}\mathbf{E}_i - \mathbf{f}_k^T\frac{\partial \mathbf{A}_i}{\partial q_i}\mathbf{F}_i - \mathbf{G}_i^T\mathbf{A}_{i-1}\mathbf{z}_0 \tag{4}$$

$$\mathbf{D}_i = \mathbf{I}_i\mathbf{C}_i^T + \mathbf{T}_{i+1}\mathbf{D}_{i+1} \tag{5}$$

$$\mathbf{E}_i = m_i\mathbf{r}_i + \mathbf{T}_{i+1}\mathbf{E}_{i+1} \tag{6}$$

$$\mathbf{F}_i = \mathbf{r}_k\delta_{ik} + \mathbf{T}_{i+1}\mathbf{F}_{i+1} \tag{7}$$

$$\mathbf{G}_i = \mathbf{h}_k\delta_{ik} + \mathbf{G}_{i+1} \tag{8}$$

where $tr(\cdot)$ is the trace of a matrix, $\mathbf{T}_i$ is the transformation matrix, $\mathbf{A}_i$, $\mathbf{C}_i$ are global position and acceleration transformation matrices, $\mathbf{I}_i$ is the inertia matrix for link i, $\mathbf{D}_i$ is the recursive inertia and Coriolis matrix, $\mathbf{E}_i$ is the recursive vector for gravity torque calculation, $\mathbf{F}_i$ is the recursive vector for external force torque calculation, $\mathbf{G}_i$ is the recursive vector for external moment torque calculation, $\mathbf{g}$ is the gravity vector, m_i is the mass of link i, $\mathbf{r}_i$ is the center of mass of link i, $\mathbf{f}_k = \begin{bmatrix} 0 & f_{ky} & f_{kz} & 0 \end{bmatrix}^{\mathrm{T}}$ is the external force applied on link k, $\mathbf{r}_k$ is the position of the external force in the local frame k, $\mathbf{h}_k = \begin{bmatrix} h_x & 0 & 0 & 0 \end{bmatrix}^{\mathrm{T}}$ is the external moment applied on link k, $\mathbf{z}_0 = \begin{bmatrix} 0 & 0 & 1 & 0 \end{bmatrix}^{\mathrm{T}}$ is for a revolute joint, $\mathbf{z}_0 = \begin{bmatrix} 0 & 0 & 0 & 0 \end{bmatrix}^{\mathrm{T}}$ is for a prismatic joint, δ_{ik} is Kronecker delta, and the starting conditions are $\mathbf{D}_{n+1} = [\mathbf{0}]$, $\mathbf{E}_{n+1} = \mathbf{F}_{n+1} = \mathbf{G}_{n+1} = [\mathbf{0}]$.

3 Motion Capture Experiments

Motion capture experiment was performed for validation and was approved by the internal review board at Texas Tech University. 20 subjects were recruited for the study. Among them, two were discarded because of incomplete capture data.

3.1 Participants. The subjects were chosen for the 50th percentile stature and body mass. Participants were all male (age: 23.07 ± 1.64 years; height: 175.46 ± 4.93 cm; body mass: 71.77 ± 5.42 kg, where $\pm$ means standard deviation). All subjects were physically and mentally sound and signed informed consent form.

3.2 Data Collection. Optical sensor based motion capture system was used. The system included 7 Eagle-4 camera system (Motion Analysis Corporation, CA). Each camera has 4-megapixel resolution with maximum 500 fps (frames per second). A 3.04×3.04 m^2 area was selected for the delivery task with cameras surrounding at a height of around 2.74 m. 52 retroreflective markers were placed on subjects' body. The markers were placed such that the markers move as little as possible on the body followed the protocol developed by Cloutier et al. [32]. Stature and body mass were recorded for each participant before experiment.

Before experiment started, participants were asked to walk five steps ahead from the initial position. Depending on the step length, the table was set to be in an appropriate distance to the subject's final step. Each participant was requested to finish the following tasks in order: (1) Stand in parallel feet behind box; (2) pick the box up to a comfortable waist height; (3) walk five steps starting from the left leg including initial transition step, three intermediate carrying steps, and final transition step; (4) stand in front of a 0.5 m height table; and (5) unload the box on the table as seen in Fig. 2. The same procedure was repeated 3 times for each subject.

3.3 Data Processing. GEBOD, a regression-based interactive utility [29], was used to generate each subject's body segment lengths, centers of mass, and inertial properties.

All markers were labeled and smoothed in Cortex (Motion Analysis Corporation, CA). Three-dimensional coordinates of the markers were converted to two dimension and the marker positions were used to calculate intended joint angles. Spine, right shoulder, right elbow, right hip, and right knee joint angles were calculated

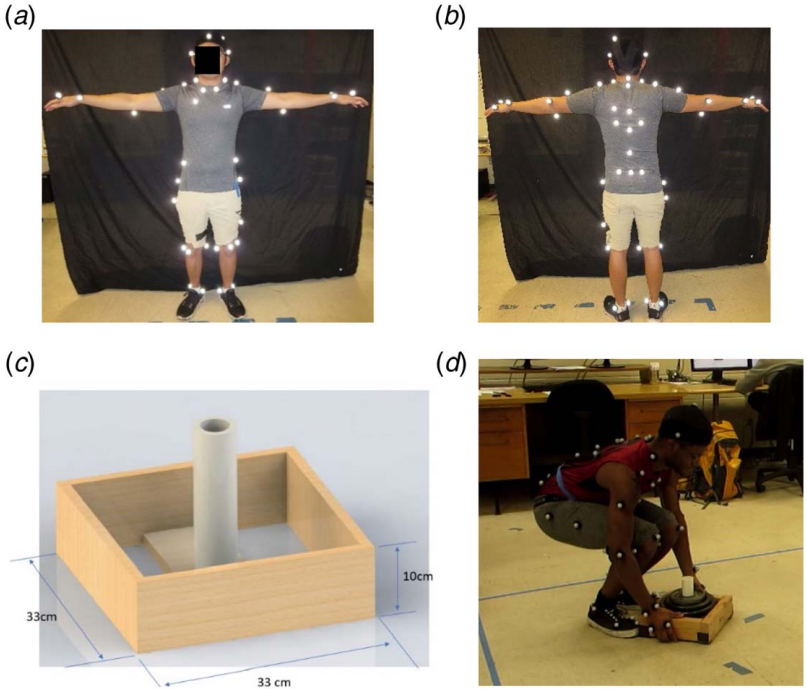

Fig. 2 Experimental setup: (*a*) marker placement protocol front view; (*b*) marker placement protocol back view; (*c*) box dimension and weight, without external load: 2.36 kg, with external load: 10.16 kg; and (*d*) experiment environment, where the average distance between initial and final position is 2.4 m and the table height of the final position from ground is 0.5 m

from motion capture data for each subject. Average and standard deviation were then calculated for all 18 subjects.

4 Single Task-Based Optimization Formulation

A whole delivery task in this study includes lifting, an initial transition, three carrying steps, a final transition, and an unloading subtask. In the single task-based formulation one single optimization is formulated for the whole task. The initial and final lifting postures, initial and final unloading postures, foot step lengths, time durations are all given from experiments. The design variables are cubic B-spline control points ($\mathbf{P}$) of joint angle profiles. The objective function J is defined by the time integral of the square of all normalized joint torques:

$$J(\mathbf{P}) = \sum_{i=4}^{n} \int_{t=0}^{T} \left[\frac{\tau_i(\mathbf{P})}{\tau_i^U - \tau_i^L} \right]^2 \mathrm{d}t \tag{9}$$

where n is the number of DOF, T is the total time of the whole delivery task, τ_i^U is the upper torque limit for ith joint, and τ_i^L is the lower torque limit.

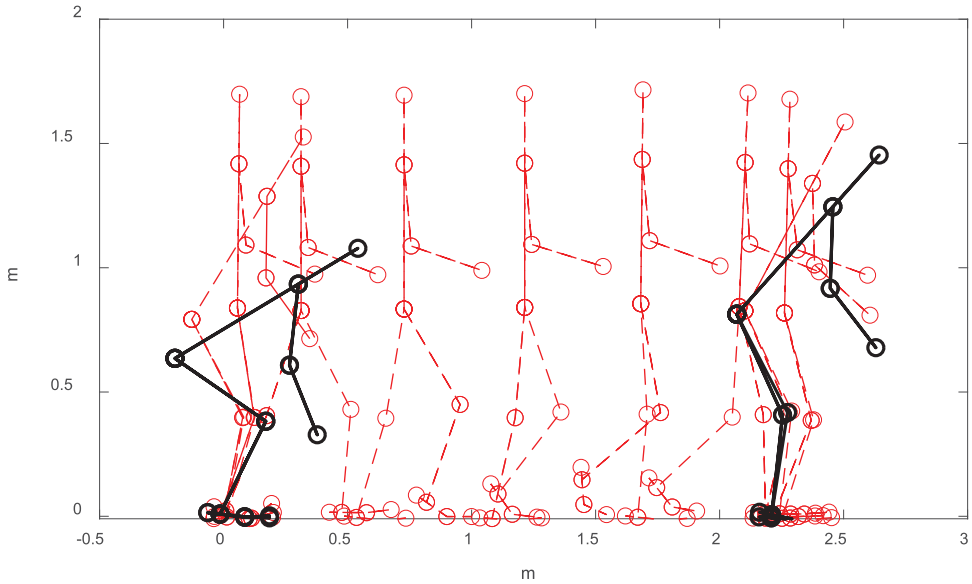

Fig. 3 Predicted optimal delivery motion snapshots for a 10.16 kg box

The single task-based optimization for the box delivery is subject to the following constraints:

Joint angle limits

$$\mathbf{q}^L \le \mathbf{q}(t) \le \mathbf{q}^U \tag{10}$$

where $\mathbf{q}$ is the joint angle profile, $\mathbf{q}^L$ and $\mathbf{q}^U$ are the lower and upper bounds, respectively. The joint angle limits are obtained from literature [33].

Joint torque limits

$$\boldsymbol{\tau}^L \le \boldsymbol{\tau}(t) \le \boldsymbol{\tau}^U \tag{11}$$

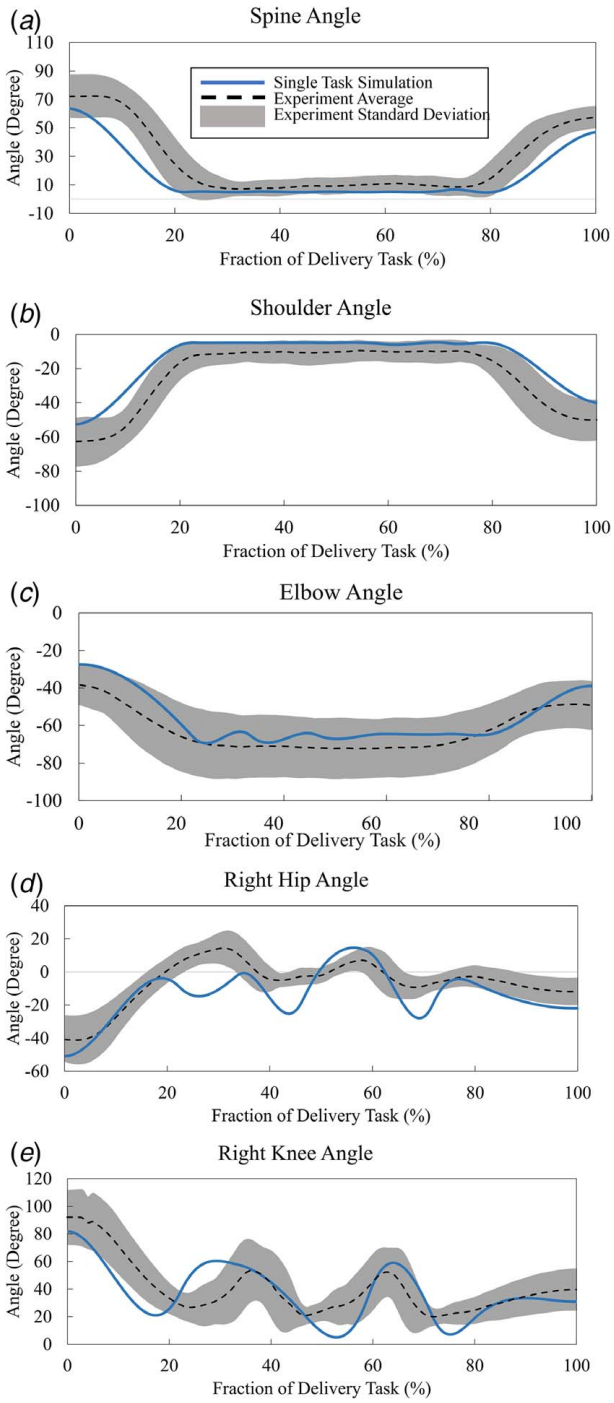

Fig. 4 Joint angle profiles for deliver motion from the simulation model and experiments: (*a*) spine, (*b*) shoulder, (*c*) elbow, (*d*) right hip, and (*e*) right knee

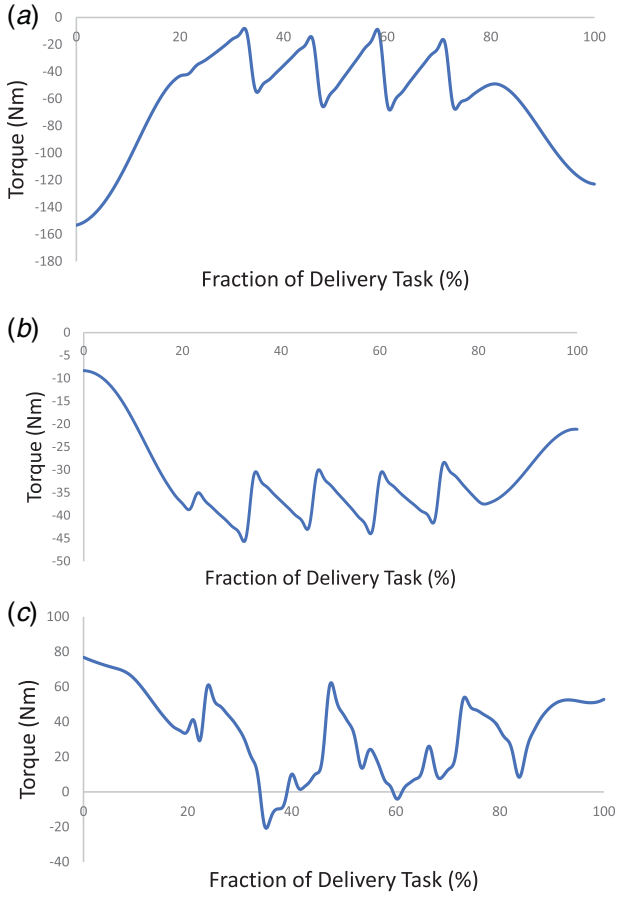

Fig. 5 Joint torque profiles for deliver motion from the simulation model: (*a*) spine, (*b*) shoulder, and (*c*) right hip

where $\boldsymbol{\tau}^L$ and $\boldsymbol{\tau}^U$ are the lower and upper joint torque bounds, respectively. The torque limits are obtained from literature [34].

In addition, the feet contacting positions are given from experiments

$$p_{foot}(\mathbf{q},\ t) = p^E_{foot}(t) \tag{12}$$

where p_{foot} is the calculated foot position from the 2D skeletal model, and p^E_{foot} is the measured foot position based on the mean experimental step lengths.

While the foot is in contact with the ground, the height of the contacting points is zero. The other points should be above the ground and the height greater than zero

$$\begin{aligned} y_i(t) &= 0; \quad i \in \text{contact} \\ y_j(t) &\ge 0; \quad j \notin \text{contact} \end{aligned} \tag{13}$$

where i is the point index on foot which is contacting the ground [33].

Balance must be considered during the box delivering process. This is the zero moment point (ZMP) constraint

$$p_{ZMP}(\mathbf{q},\ t) \in \text{FSR} \tag{14}$$

where p_{ZMP} is the ZMP location, and FSR represents the foot support region.

Collision avoidance between box and body

$$d(\mathbf{q},\ t) \ge r_1 + r_2 \tag{15}$$

where d is the calculated distance between the hand and the circle center on the body segment representing the body thickness, r_1 is half of the box width, and r_2 is the radius of the circle of the body segment.

Table 1 RMSE and Pearson correlation coefficient (r) averaged across 18 subjects, values are represented as mean (standard deviation)

	Spine	Shoulder	Elbow	Right hip	Right knee
RMSE	15.47 (5.52)	14.08 (5.92)	15.28 (6.25)	13.93 (1.95)	20.79 (4.15)
r	0.91 (0.06)	0.92 (0.06)	0.74 (0.41)	0.69 (0.11)	0.57 (0.12)

Knee flexion at mid-swing is around 60 deg to avoid foot drag motion

$$|q_{knee}(t) - 60 \text{ deg}| \leq 10 \text{ deg}; \qquad t = t_{midswing} \tag{16}$$

where $t_{midswing}$ is the experimental mean value determined at 75% of the gait cycle [33].

The joint angle differences between the skeletal model and the experiment are constrained in a small range $\varepsilon = 10$ deg at initial and final lifting/unloading postures, where $\mathbf{q}^E$ is the experimental joint angle

$$|\mathbf{q}(t) - \mathbf{q}^E(t)| \leq \varepsilon; \; t = 0, t^{final}_{lifting}, t^{initial}_{unloading}, T \tag{17}$$

Finally, the upper body joint angles are constrained to the experimental mean values during carrying motion

$$|\mathbf{q}_{upper}(t) - \bar{\mathbf{q}}^E_{upper}(t)| \leq \varepsilon; \quad t \in t_{carrying} \tag{18}$$

where $\bar{\mathbf{q}}^E_{upper}$ is the experimental mean and $\varepsilon = 10$ deg.

5 Simulation Results

The sequential quadratic programming algorithm in SNOPT [35] is used to solve the optimization problem. Solving the single task-based optimization problem based on the input data from experiments (mean values from all subjects) yields simulation results. Figure 3 shows the snapshots for the optimal delivery motion. Figure 4 shows the joint angle profiles' comparison with the experimental results. The joint torque profiles are shown in Fig. 5. This optimization problem has 210 design variables, 2767 constraints, 15 control points for each DOF, and 54.49 s CPU time. Table 1 lists the root-mean-square-error (RMSE) and Pearson's correlation coefficient (r) for comparing the predicted and experimental joint angle profiles.

In Fig. 3, it shows the snapshots of the deliver motion. In Fig. 4, the predicted joint angles (spine, shoulder, elbow, right knee) lie within the standard deviation of the mean for the major portion of the motion and also follow the similar trend as the experimental mean, indicating reasonable agreement with the experimental results. For the right hip angle in Fig. 4(*d*), the carrying motion has similar trend as the experimental mean but is outside the standard deviation. The minimum values are outside of the experimental standard deviation. This is because we did not impose experimental boundary conditions for carrying simulation. For lifting and unloading motions, although the experimental boundary constraints are imposed, the spine and shoulder joint angles are still partially outside the standard deviation between the boundaries as seen in Figs. 4(*a*) and 4(*b*). The spine, shoulder, right hip joint torque profiles in Fig. 5 show repeatable patterns during carrying motion as expected.

6 Discussion and Conclusion

In this study, single task optimization-based method has been presented to predict the box delivery motion. A motion capture experiment is conducted to collect kinematic data for box delivery validation. In addition, simulation results are compared with the experimental data. Torque limits (joint strength [34]) are considered as one of the constraints in the optimization formulation. If the optimization successfully converges, i.e., the torque limit constraints are not violated, the subject will not get injured in joint torque space. Therefore, joint torque limits are important for predicting potential injuries for workers. This has been demonstrated for the maximum weight lifting prediction by considering dynamic joint strength [36].

It can be seen from Table 1 that the simulation method matches well with the experimental results based on the RMSE and Pearson's coefficient. The major advantage of single task-based method is that the boundary conditions between subtasks are avoided and the same cost function is considered throughout the entire motion. In future, we will investigate the subtask-based optimization approach, and simulate more complicated three-dimensional motions.

Acknowledgment

This research is supported by NSF projects (CBET 1849279 and 1703093). We thank Adrian Harvey, undergraduate researcher from Texas Tech University, for helping in experimental data collection.

Conflict of Interest

There are no conflicts of interest.

Data Availability Statement

The datasets generated and supporting the findings of this article are obtainable from the corresponding author upon reasonable request. The authors attest that all data for this study are included in the paper.

References

[1] Liberty Mutual Insurance, Liberty Mutual Workplace Safety Index, https://www.libertymutualgroup.com/about-liberty-mutual-site/news-site/Documents/2019%20Workplace%20Safety%20Index.pdf, Accessed September 1, 2019.

[2] Harari, Y., Bechar, A., and Riemer, R., 2016, "An Investigation of Workplace Design and the Worker's Anthropometrics Influence on Work Pace During Manual Material Handling Tasks," Proceedings of 2016 Human Factors and Ergonomics Society Annual Meeting, Washington, DC, Sept. 19–23, vol. 60, No. 1, pp. 727–728.

[3] Saidouni, T., and Bessonnet, G., 2003, "Generating Globally Optimised Sagittal Gait Cycles of a Biped Robot," Robotica, **21**(2), pp. 199–210.

[4] Huang, C., Sheth, P. N., and Granata, K. P., 2005, "Multibody Dynamics Integrated With Muscle Models and Space-Time Constraints for Optimization of Lifting Movements," Proceedings of 2005 ASME International Design Engineering Technical Conference s and Computers and Information in Engineering Conference, Long Beach, CA, pp. 391–398.

[5] Davy, D. T., and Audu, M. L., 1987, "A Dynamic Optimization Technique for Predicting Muscle Forces in the Swing Phase of Gait," J. Biomech., **20**(2), pp. 187–201.

[6] Chow, C. K., and Jacobson, D. H., 1971, "Studies of Human Locomotion via Optimal Programming," Math. Biosci., **10**(3–4), pp. 239–306.

[7] Bessonnet, G., Sardain, P., and Chesse, S., 2002, "Optimal Motion Synthesis—Dynamic Modeling and Numerical Solving Aspects," Multibody Syst. Dyn., **8**(3), pp. 257–278.

[8] Bessonnet, G., Chesse, S., and Sardain, P., 2004, "Optimal Gait Synthesis of a Seven-Link Planar Biped," Int. J. Robot. Res., **23**(10–11), pp. 1059–1073.

[9] Neptune, R. R., Kautz, S. A., and Zajac, F. E., 2001, "Contributions of the Individual Ankle Plantar Flexors to Support, Forward Progression and Swing Initiation During Walking," J. Biomech., **34**(11), pp. 1387–1398.

[10] Yamaguchi, G. T., and Zajac, F. E., 1990, "Restoring Unassisted Natural Gait to Paraplegics via Functional Neuromuscular Stimulation—a Computer-Simulation Study," IEEE Trans. Biomed. Eng., **37**(9), pp. 886–902.

[11] Channon, P. H., Hopkins, S. H., and Pham, D. T., 1992, "Derivation of Optimal Walking Motions for a Bipedal Walking Robot," Robotica, **10**(2), pp. 165–172.

[12] Koopman, B., Grootenboer, H. J., and Dejongh, H. J., 1995, "An Inverse Dynamics Model for the Analysis, Reconstruction and Prediction of Bipedal Walking," J. Biomech., **28**(11), pp. 1369–1376.

[13] Chevallereau, C., and Aoustin, Y., 2001, "Optimal Reference Trajectories for Walking and Running of a Biped Robot," Robotica, **19**(5), pp. 557–569.

[14] Bessonnet, G., Seguin, P., and Sardain, P., 2005, "A Parametric Optimization Approach to Walking Pattern Synthesis," Int. J. Robot. Res., **24**(7), pp. 523–536.

[15] Ren, L., Jones, R. K., and Howard, D., 2007, "Predictive Modeling of Human Walking Over a Complete Gait Cycle," J. Biomech., **40**(7), pp. 1567–1574.
[16] Kim, H. J., Wang, Q., Rahmatalla, S., Swan, C. C., Arora, J. S., Abdel-Malek, K., and Assouline, J. G., 2008, "Dynamic Motion Planning of 3D Human Locomotion Using Gradient-Based Optimization," ASME J. Biomech. Eng., **130**(3), p. 031002.
[17] Farahani, S. D., Andersen, M. S., de Zee, M., and Rasmussen, J., 2016, "Optimization-Based Dynamic Prediction of Kinematic and Kinetic Patterns for a Human Vertical Jump From a Squatting Position," Multibody Syst. Dyn., **36**(1), pp. 37–65.
[18] Ackermann, M., and van den Bogert, A. J., 2010, "Optimality Principles for Model-Based Prediction of Human Gait," J. Biomech., **43**(6), pp. 1055–1060.
[19] de Groote, F., Kinney, A. L., Rao, A. V., and Fregly, B. J., 2016, "Evaluation of Direct Collocation Optimal Control Problem Formulations for Solving the Muscle Redundancy Problem," Ann. Biomed. Eng., **44**(10), pp. 2922–2236.
[20] Hirai, K., 1999, "The Honda Humanoid Robot: Development and Future Perspective," Ind. Robot, **26**(4), pp. 260–266.
[21] Azevedo, C., Poignet, P., and Espiau, B., 2004, "Artificial Locomotion Control: From Human to Robots," Robot. Auton. Syst., **47**(4), pp. 203–223.
[22] Forster, E., 2004, "Predicting Muscle Forces in the Human Lower Limb During Locomotion," Ph.D. dissertation, University of Ulm, Germany.
[23] Arnold, A. S., Thelen, D. G., Schwartz, M. H., Anderson, F. C., and Delp, S. L., 2007, "Muscular Coordination of Knee Motion During the Terminal-Swing Phase of Normal Gait," J. Biomech., **40**(13), pp. 3314–3324.
[24] Hull, D. G., 1997, "Conversion of Optimal Control Problems Into Parameter Optimization Problems," J. Guid. Control Dyn., **20**(1), pp. 57–60.
[25] Shourijeh, M. S., Smale, K. B., Potvin, B. M., and Benoit, D. L., 2016, "A Forward-Muscular Inverse-Skeletal Dynamics Framework for Human Musculoskeletal Simulations," J. Biomech., **49**(9), pp. 1718–1723.
[26] Thelen, D. G., Anderson, F. C., and Delp, S. L., 2003, "Generating Dynamic Simulations of Movement Using Computed Muscle Control," J. Biomech., **36**(3), pp. 321–328.
[27] Thelen, D. G., and Anderson, F. C., 2006, "Using Computed Muscle Control to Generate Forward Dynamic Simulations of Human Walking From Experimental Data," J. Biomech., **39**(6), pp. 1107–1115.
[28] Wagner, D. W., Kirschweng, R. L., and Reed, M. P., 2009, "Foot Motions in Manual Material Handling Transfer Tasks: A Taxonomy and Data From an Automotive Assembly Plant," Ergonomics, **52**(3), pp. 362–383.
[29] Cheng, H., Obergefell, L., and Rizer, A., 1994, "Generator of Body (GEBOD) Manual," Armstrong Laboratory, Wright-Patterson Air Force Base, Dayton, OH, Technical Report, AL. CF-TR-1994–0051.
[30] Denavit, J., and Hartenberg, R. S., 1955, "A Kinematic Notation for Lower Pair Mechanisms Based on Matrices," ASME J. Appl. Mech., **22**(2), pp. 215–221.
[31] Xiang, Y., Arora, J. S., and Abdel-Malek, K., 2009, "Optimization-Based Motion Prediction of Mechanical Systems: Sensitivity Analysis," Struct. Multidiscip. Optim., **37**(6), pp. 595–608.
[32] Cloutier, A., Boothby, R., and Yang, J., 2011, "Motion Capture Experiments for Validating Optimization-Based Human Models," Proceedings of HCI-3rd International Conference on Digital Human Modeling, Orlando, FL, pp. 59–68.
[33] Xiang, Y., Arora, J. S., Rahmatalla, S., and Abdel-Malek, K., 2009, "Optimization-Based Dynamic Human Walking Prediction: One Step Formulation," Int. J. Numer. Methods Eng., **79**(6), pp. 639–772.
[34] Xiang, Y., Arora, J. S., Chung, H. J., Kwon, H. J., Rahmatalla, S., Bhatt, R., and Abdel-Malek, K., 2012, "Predictive Simulation of Human Walking Transitions Using an Optimization Formulation," Struct. Multidiscip. Optim., **45**(5), pp. 759–772.
[35] Gill, P. E., Murray, W., and Saunders, M. A., 2002, "SNOPT: An SQP Algorithm for Large-Scale Constrained Optimization," SIAM J. Optim., **12**(4), pp. 979–1006.
[36] Rakshit, R., Xiang, Y., and Yang, J., 2020, "Dynamic-joint-strength-based Two-Dimensional Symmetric Maximum-Weight Lifting Simulation: Model Development and Validation," Proceedings of the Institution of Mechanical Engineers, Part H: Journal of Engineering in Medicine, vol. 234, no. 7, pp. 660–673.